Observation of a charge delocalization from Se vacancies in Bi_2Se_3: a positron annihilation study of native defects

I. Unzueta,[1,2,*] N. Zabala,[1,3,4,†] V. Marín-Borrás,[5,‡] V. Muñoz-Sanjosé,[5,§] J. A. García,[6,2,¶] and F. Plazaola[1,**]

[1] *Department of Electricity and Electronics, University of the Basque Country UPV/EHU, 48940 Leioa, Spain*
[2] *BCMaterials, University of Basque Country UPV/EHU, 48940 Leioa, Spain*
[3] *Materials Physics Center (MPC) CSIC-UPV/EHU, 20018 Donostia-San Sebastián, Spain*
[4] *Donostia International Physics Center (DIPC), 20018 Donostia-San Sebastián, Spain*
[5] *Departamento de Física Aplicada, Universitat de Valencia, 46100 Burjassot, Valencia, Spain*
[6] *Department of Applied Physics II, University of the Basque Country UPV/EHU, 48940 Leioa, Spain*

By means of positron annihilation lifetime spectroscopy, we have investigated the native defects present in Bi_2Se_3, which belongs to the family of topological insulators. We experimentally demonstrate that selenium vacancy defects (V_{Se1}) are present in Bi_2Se_3 as-grown samples, and that their charge is delocalized as temperature increases. At least from 100 K up to room temperature both V^0_{Se1} and V^+_{Se1} charge states coexist. The observed charge delocalization determines the contribution of V_{Se1} defects to the *n*-type conductivity of Bi_2Se_3. These findings are supported by theoretical calculations, which show that vacancies of non-equivalent Se1 and Se2 selenium atoms are clearly differentiated by positron annihilation lifetime spectroscopy, enabling us to directly detect and quantify the most favorable type of selenium vacancy. In addition to open-volume defects, experimental data indicate the presence of defects that act as shallow-traps suggesting that more than one type of native defects coexist in Bi_2Se_3. As will be discussed, the presence of a dislocation density around 10^{10} cm^{-2} could be the source of the detected shallow traps. Understanding the one-dimensional defects and the origin of the charge delocalization that leads Bi_2Se_3 to be a *n*-type semiconductor will help in the development of high quality topological insulators based on this material.

PACS numbers: 78.70.Bj, 61.72.jd

I. INTRODUCTION

Topological insulator (TIs) behave like an insulator in the bulk, whereas it exhibits exotic metallic surface states that are protected by time-reversal symmetry[1–13]. These surface states exhibit a Dirac cone-like electronic structure, with a linear energy dispersion that falls within the bulk energy gap. Moreover, the momentum and the spin of electrons are locked in a way that electrons with opposite momentum have opposite spins[14–16]. Due to the spin texture of the surface states, TI have attracted a considerable interest in condensed matter community as potential candidates for applications in spintronics and quantum computing[17,18].

However, most of TI compounds are not perfect insulators in bulk and charge transport is dominated by bulk carriers, being the main drawback for developing TI-based devices for the aforementioned applications. Surface sensitive techniques as angle-resolved photoemission spectroscopy[19,20] and scanning tunneling microscopy[21,22] can be used to access the surface states regardless of the electrical character of the bulk. Besides, optical and transport techniques can be used to uncover the physics of surface states. Nevertheless, the non-desired bulk conductance hinders the realization of TIs in which the transport properties would be mainly dominated by the contribution of the surface states[23–25]. In order to reduce the bulk conductance and enhance the contribution of the surface states, several methods such as gating[26–28], size-reducing[29–32] and doping[33–36] have been employed.

One of the most extensively studied TI compound is Bi_2Se_3. This compound has a single Dirac cone at the Γ point ($k = 0$) in the surface Brillouin zone. The energy gap of this compound is a topologically non-trivial gap with a value of 350 meV, higher than room temperature energy scale. This value of the energy gap and the relatively simple surface states make Bi_2Se_3 a good candidate for potential future applications. Despite these promising features, the bulk of Bi_2Se_3 is not a perfect insulator and exhibits a large bulk carrier concentration that becomes it in a *n*-type material. Thus, the Fermi level is shifted to the conduction band, making difficult the characterization of the surface transport properties. Obtaining an intrinsic TI material involves getting a controllable electronic structure in order to minimize the spurious bulk contribution. The main reason claimed for the unintentional intrinsic *n*-type doping of TIs, and in particular, of Bi_2Se_3, are intrinsic defects, such as vacancies and anti-sites[37–39]. Hence, a qualitative and quantitative investigation of the native defects in TIs is crucial in order to be able to tune the electronic structure towards an intrinsic TI. As a result, several investigations have been carried out focused on uncovering the most favorable na-

tive defects in Bi_2Se_3.

Most studies related with intrinsic defects in Bi_2Se_3, have been conducted in the frame of theoretical studies (e.g., Ref. [39–42]) and unfortunately only a few experimental reports can be found[38,43–46]. Theoretical investigations present non-consensus results because different types of the most favorable defects are predicted. Moreover, experimentally observed defects are not the same in all cases and most of the theoretical calculations predict a single type of defect to be the most favorable. Furthermore, both the calculated and experimentally obtained charge state of defects are also different[40,42–44].

In some of the previous works the defect formation energies are also calculated[39–42,45]. All the same, the interpretation varies significantly depending on the work and on the employed theoretical method. Thus, an experimental tool capable to measure directly the native defects seems to be of interest in order to determine which of the theoretical predictions are the most adequate. The shortage of experimental studies on the direct detection of native defects is partly due to the existence of few experimental tools capable to detect defects at atomic scale, (e.g., nuclear magnetic resonance[46], resistive methods[43,45] and microscopy methods[38,44]).

An additional technique capable to detect directly the structural defects is positron annihilation lifetime spectroscopy (PALS). This technique has been widely used over decades and it is a powerful tool for defect characterization in semiconductors[47]. The positron lifetime is directly related with the electronic density of the material. Crystal imperfections such as vacancy defects alter significantly the surrounding electronic density and the positron lifetime varies when trapped in such defects. In semiconductors, PALS also provides information about the charge state of defects[47].

Very little work has been carried out by using PALS as defect detection technique for TIs. Devidas *et al.* Ref. [48], presents a comparative study between PALS and magnetotransport, where PALS measurements were carried out at room temperature, suggesting the presence of selenium vacancy defects. However, a temperature dependent PALS study and the determination of the most probable charge state of defects remains unperformed. The temperature evolution of the average positron lifetime might determine the native defects of Bi_2Se_3, asserts their charge state and also indicate the possible coexistence of more than one type of defect. Investigating the variation of the charge state of defects is crucial for a better understanding of the origin of bulk conductance and also for tuning the electronic properties in order to be useful for applications.

In the present work we have investigated the native defects in Bi_2Se_3 topological insulator by means of PALS, on as-grown samples as well as, in order to modify the defect concentration, on heat-treated samples. The obtained results have been analyzed in the frame of theoretical trapping models. Additionally, we have calculated the expected positron lifetime for a defect-free structure and for a structure containing different type of vacancy defects by using the Atomic Superposition Approximation method (ATSUP).

Our theoretical study shows that non-equivalent selenium vacancies in Bi_2Se_3 are clearly differentiated by positron annihilation lifetime, allowing the determination of the most favorable type of selenium vacancies. These findings are supported by our experimental results obtained on heat-treated samples. Additionally, we observe that the charge state of V_{Se1} varies as temperature increases and we will show that neutral and positively charged states coexist in Bi_2Se_3. The observed charge delocalization quantifies the contribution of V_{Se1} to the n-type conductivity of Bi_2Se_3 as neutrally charged vacancies ionize towards positively charged ones with increasing temperature. Moreover, in coexistence with selenium vacancies, defects that acts as shallow traps (ST) are also present in Bi_2Se_3. Our experimental results are compatible with the assumption that the source of ST are dislocations. As the dislocations are associated with one-dimensional fermionic excitations in a TI[49] and the fact that their strain can be used to enhance or destroy the Dirac states[50,51], the determination of the dislocation density in the as-grown samples could be fundamental to develop high quality TI compounds.

II. EXPERIMENTAL METHODS

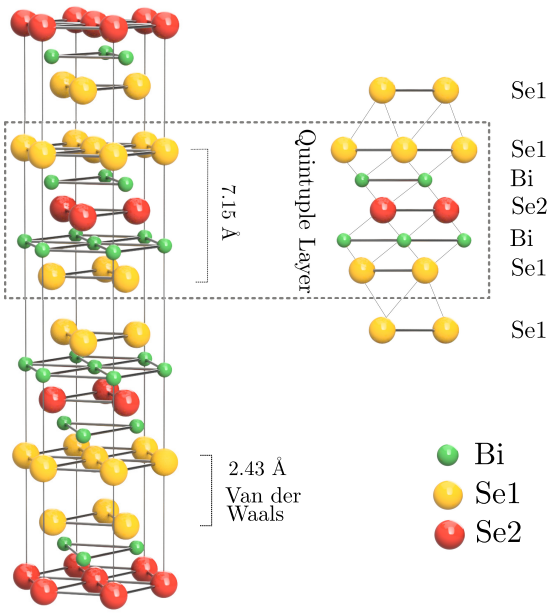

FIG. 1. (Color Online). Crystal structure of Bi_2Se_3. The quintuple layer (QL) is formed by two equivalent bismuth atoms in a equivalent position and three selenium atoms which are in two non-equivalent selenium positions denoted as Se1 and Se2. Se1 atoms are located into atomic layers that are bound by van der Waals forces. Se2 atoms are arranged within the QL in which atoms are coupled by covalent forces.

Single crystals of Bi_2Se_3 were grown by using the Bridgman method. Stoichiometric quantities of 5N Bismuth and Selenium were melted together in a vacuum sealed quartz ampoule, in order to synthesize a polycrystalline ingot. This polycrystalline ingot was the source material for the growth by the Brigdman method in which the melted material was subjected to a cooling process under well-defined conditions regarding temperature gradient and growth rate.

Fig. 1 shows the crystal structure of Bi_2Se_3. This compound has a tetradymite crystal structure and the rhombohedral layered structure is formed by quintuple layers (QL)[52]. Each QL consist of five hexagonal closed-packed atomic layers (Se1-Bi-Se2-Bi-Se1), with non-equivalent Se1 and Se2 selenium atoms and two electronically equivalent positions for the Bi atoms. The coupling between atomic layers within a QL is strong, while each QL is bound by van der Waals (VDW) forces.

PALS experiments have been performed using a fast-fast timing coincidence spectrometer with a full width at half maximum resolution of 250 ps. The detectors are equipped with plastic scintillators from Saint-Gobain (BC-422) and Hamamatsu photomultiplier tubes (H1949-50) suited in a horizontal position (collinear geometry). Measurements have been taken in the 15 K - 315 K temperature range. The used positron source was a 15 μCi ^{22}NaCl encapsulated between 7.5 μm Kapton foils and sandwiched by a pair of identical samples. In order to ensure the same structural and compositional properties, the measured samples were selected from the same location of the Bi_2Se_3 single crystal. Additionally, several pieces along the sample were measured, resulting on identical PALS spectra. Positron data have been collected with more than 3×10^6 counts and analyzed with the POSITRONFIT code[53].

All spectra have been analyzed after subtracting the source contribution, which consists of two different components. The lifetime related with the first one is typically around of 1500 ps[54,55] and its intensity in all spectra has been about 2.5 %. Although the origin of this component is not entirely clear, it is supposed to be related with the positronium formation on the surface. Indeed, recent works demonstrate the existence of positron surface states on topological insulators[56] The second lifetime component is related with the positron annihilation in Kapton, which is 382 ps[57,58]. The calculated intensity[59] for the positrons annihilating in Kapton has been 25 %, whereas the experimentally obtained value of the intensity that minimizes the chi-square (χ^2) in the spectra has been 24.5 %.

In order to avoid selenium evaporation, the heat treatments of the Bi_2Se_3 samples have been performed at 9×10^2 mbar pressure and under high purity argon atmosphere. The samples have been kept at 423 K and 473 K during 30 minutes to ensure thermal equilibrium and afterwards they have been quenched into ice water at the triple point. Scanning electron microscope micrographs have revealed that no oxidation process has happened. Additionally, the composition have been checked by means of SEM after heat treatments and no compositional change has been observed. Throughout this work we have labeled the three states of samples: as-grown, Q423 and Q473 respectively.

III. COMPUTATIONAL METHOD

For a better interpretation of lifetimes extracted from PALS measurements, we have carried out calculations of the positron lifetime in Bi_2Se_3 using a two-component density functional theory[60,61]. The positron annihilation rate λ, i.e. the inverse of the positron lifetime, is given by the overlap of the positron density $n_+(\mathbf{r})$ and the electron density of the crystal $n_-(\mathbf{r})$ as

$$\lambda = \frac{1}{\tau} = \pi c r_0^2 \int n_+(\mathbf{r}) n_-(\mathbf{r}) \gamma(\mathbf{r}) \mathrm{d}\mathbf{r}, \tag{1}$$

where c is the speed of light in vacuum, r_0 the classical electron radius and $\gamma(\mathbf{r})$ the so-called enhancement factor that comprises the enhanced electron density due to the positron Coulombic attraction. The positron lifetimes for perfect and defected lattices have been calculated by using the ATSUP method[62]. This approximation is widely used and the calculated lifetimes are in a quite good agreement with measured positron lifetimes in metals and semiconductors[63–66]. The electron density $n_-(\mathbf{r})$, is constructed by adding individual atomic n_-^i charge densities around $\mathbf{R_i}$ atomic positions, over all the occupied atomic states:

$$n_-(\mathbf{r}) = \sum_i n_-^i(|\mathbf{r} - \mathbf{R_i}|). \tag{2}$$

The felt potential by the positron, $V_+(\mathbf{r})$, is constructed as

$$V_+(\mathbf{r}) = V_c(\mathbf{r}) + V_{corr}[n_-(\mathbf{r})], \tag{3}$$

where $V_c(\mathbf{r})$ is the Coulomb potential of the entire crystal and $V_{corr}[n_-(\mathbf{r})]$ the positron-electron correlation potential, which depends on the electron density. The Schrödinger equation is solved iteratively using a numerical relaxation method[67] to obtain the positron wave function and its energy eigenvalue.

The local density approximation (LDA) has been used to calculate both the correlation potential and enhancement factor, which depends only on the local electron density on the positron site. We have used the parametrization of $\gamma(\mathbf{r})$ introduced by Boronski and Nieminen (BN)[61]. Recently, Barbiellini *et al*[68] have shown that calculations performed using the parameter-free generalized gradient approximation (PF) GGA, provides more accurate values comparing with LDA. However, in our case LDA itself seems enough to give account

of the experimentally measured lifetimes.The simulation has been carried out using a supercell method in which periodic boundary conditions are considered. We have checked that the difference in the size of the supercell does not affect to the calculated lifetimes. The supercell considered for vacancy calculations was a $4 \times 4 \times 4$ expansion of the primitive cell, containing 320 atoms. The orthorhombic unit cell has been constructed by using the lattice parameters from Ref. [52]: $a = b = 4.143$ Å and $c = 28.636$ Å.

IV. POSITRON TRAPPING AT DEFECTS

When a positron enters in a solid, it loses energy until reaches the thermal equilibrium. Thermalization is followed by diffusion through the solid, until the positron annihilates with a surrounding electron. In a defect-free lattice, the positron annihilates from the delocalized state (i.e. Bloch state) at an average rate λ_b or with a characteristic lifetime τ_b. However, solids have imperfections in their lattice, such as vacancies, dislocations or antisite defects that may act as positron traps. The trapping occurs when a positron turns from the Bloch state into a localized state within a defect (i.e. the positron wave function is localized at the defect). The κ_d trapping rate of a defect is proportional to the defect concentration C_d as $\kappa_d = \mu_d C_d$[69]. The μ_d parameter is the specific trapping coefficient of the defect and it depends on the type of defect and on the surrounding lattice[70,71].

When a sample contains different positron states (bulk and defect states) where positrons may annihilate, the statistically strongest parameter obtained from the PALS spectrum is the average positron lifetime $\bar{\tau}$, which is composed by the different positron annihilation contributions coming from the different positron states in the material. The contributions are weighted with individual I_i intensities, so that

$$\bar{\tau} = \sum_i I_i \tau_i, \tag{4}$$

where τ_i is the lifetime related with i-th defect. Vacancies are the most important traps for positrons in semiconductors. Due to the lack of the positive ion, vacancies act as deep traps for positrons. Vacancies are characterized by an open volume with an electron density lower than the one corresponding to the perfect lattice and, as a consequence, they exhibit longer positron lifetimes. Additionally, depending on the charge state of defects, the annihilation parameters change.

Positron trapping at positively charged vacancies is practically forbidden because the Coulomb repulsion[72]. However, neutral and negatively charged vacancies are efficient positron traps. Although the trapping rate for neutral vacancies is temperature independent, for negatively charged vacancies, the long range potential induces a series of precursor Rydberg states where positrons can be trapped before getting trapped into the negative vacancy (direct transition from bulk into the deep state of vacancy is considered as negligible[72]). Besides, the κ_R trapping rate of the Rydberg states depends on temperature,

$$\kappa_R = \kappa_{R0} T^{-1/2} \tag{5}$$

where κ_{R0} is the trapping rate at a certain low temperature. This means that in negatively charged vacancies, the trapping rate of positrons also depends on temperature. Positrons trapped at precursor Rydberg states can either be trapped into the deep state of the vacancy, or be detrapped into bulk states by thermal stimulation. As a result of the previous two channels for positrons, the amount of positrons annihilating at vacancy states decreases as temperature increases. The detrapping-rate δ_R from the Rydberg states is given by

$$\delta_R = \frac{\kappa_R}{C_v^-} \left(\frac{m^* k_B T}{2\pi\hbar^2} \right)^{3/2} \exp\left(-\frac{E_R}{k_B T} \right) \tag{6}$$

where C_v^- is the concentration of negatively charged vacancies, m^* is the effective mass of the positron, k_B the Boltzmann constant, $\hbar$ the reduced Planck constant and E_R the positron binding energy at the Rydberg state[73]. Summarizing, the positron trapping process at negatively charged vacancy defects works as follows: positrons are first trapped at Rydberg states at a κ_R rate. Once they are trapped, positrons can be detrapped to a Bloch state at a δ_R rate or they can suffer a transition into a deep state of the vacancy at η rate. It is worth noting that positrons cannot escape from the deep state, but they will be annihilated at the vacancy with a well-defined rate $\lambda_v = \tau_v^{-1}$. Thus, combining trapping and the detrapping phenomena (Eq. (5) and Eq. (6)), the effective $\kappa_{v^-}^{eff}$ trapping rate of positrons at negatively charged vacancies can be written as[72]

$$\kappa_{v^-}^{eff} = \frac{\kappa_R \, \eta}{\eta + \delta_R} \tag{7}$$

$$= \frac{\kappa_{R0} T^{-1/2} \eta C_v^-}{C_v^- \eta + \kappa_{R0} \left(\frac{m^* k_B}{2\pi\hbar^2} \right)^{3/2} T \exp\left(\frac{-E_R}{k_B T} \right)} \tag{8}$$

In the case of neutral vacancies, the trapping rate does not depend on temperature and by comparing with negatively charged vacancies, the trapping coefficient μ_v^0 is expected to be about one order of magnitude smaller[72,74]. Due to the absence of long-range Coulomb tail, Rydberg states are not induced in neutral vacancies and the trapping at shallow Rydberg states is not possible. Thus, the κ_v^0 trapping rate for neutral vacancies is proportional to the μ_v^0 specific trapping-coefficient, $\kappa_v^0 = \mu_v^0 C_v^0$. Often, a temperature independent trapping rate at high temperatures is a clear evidence for the presence of neutral

vacancy defects. In fact, the different temperature dependence that exhibit negative and neutral vacancies, allows a selective detection between them.

Nevertheless, the charge state of a defect in a semiconductor can vary with temperature and the defect may be ionized. The defect ionization can be taken into account by using the Fermi statistics[75]:

$$f(\epsilon) = \frac{1}{1 + \frac{1}{g}\exp\left(\frac{\epsilon_d - \epsilon_f}{k_B T}\right)} \tag{9}$$

where g is the degeneracy factor, ϵ_d the energy of the defect level and ϵ_f the energy of the Fermi level. A change in the charge state of a vacancy modifies the specific trapping coefficient μ_v and therefore, the κ_v positron trapping becomes a combination of the trapping characteristic of each defect[76],

$$\kappa_v = \left[f(\epsilon)\mu + (1 - f(\epsilon))\mu^*\right] C_v. \tag{10}$$

Here, μ indicates the specific trapping rate related to the more negatively charged vacancy and μ^* the trapping coefficient of the more positively charged defect. If a transition occurs from negatively charged vacancies to neutral vacancies, then $\mu > \mu^*$. However, considering a charge state transition from neutral to positively charged, $\mu \gg \mu^*$ and Eq. (10) can be simplified as $\kappa \approx f(\epsilon)\mu_v^0 C_v^0$. As positively charged vacancies are no longer attractive for positrons, this fact can be also interpreted as a reduction in the concentration of the vacancies that are "seen" by positrons. Indeed, this reduction is weighted with the factor of Eq. (9).

Beyond open-volume defects, negatively charged defects without open-volume (e.g., acceptor-type impurities or anti-site defects), can also act as positron trapping centers (also called ionic traps). The trapping occurs when a positron in a delocalized state gets trapped in the Rydberg states caused by the long-range Coulomb of the defect potential[77,78]. In this case, due to the lack of open volume, the position probability density of positrons trapped at ST is extended into the bulk surrounding the ST. Thus, the expected lifetime of positrons trapped in ST is similar to that of the positrons in a Block state or in a delocalized state. Due to the small binding energy of positrons trapped at Rydberg states, the trapping only occurs below room temperature[79].

The physics governing the detrapping in non-open-volume defects is almost identical to that previously described. The activation energy of the detrapping process is equal to the binding energy E_R of positrons to Rydberg states, and the detrapping rate has the same expression as described in Eq. (6)[?] . In the case of ST, κ_R and C_v must be substituted by κ_{ion} and C_{ion} because open-volume defects and defects that act as ST have different annihilation characteristics. Overall, the effective trapping rate κ_{ion}^{eff} of non-open volume defects can be defined as[80]

$$\kappa_{ion}^{eff} = \frac{\kappa_{ion}}{1 + \delta_{ion}\tau_{ion}}, \tag{11}$$

where δ_{ion} is the detrapping rate of positrons from ST and τ_{ion} the lifetime related with ST. Since ST have similar annihilation parameters than the bulk, $\tau_{ion} = \tau_b$ can be considered. Thus, the direct detection of ST is often not possible. However, the pronounced temperature dependence of the average positron lifetime, as a result of competition between trapping at vacancies and at ST proves their presence[47].

Additionally, shallow positron trapping may also occur at defects that are characterized by a tiny open-volume, related to a small binding energy, e.g., dislocations. Although the exact mechanism of the positron trapping at dislocations is not entirely clear, several models as, viz. transition-limited trapping in dislocations[81], the diffusion-limited trapping[69], and the shallow-trap model[82] have been proposed so far. For most dislocation types in semiconductors the open volume is expected to be rather small and therefore, it is assumed that the positron lifetime trapped at dislocation lines should be almost the same as the bulk value[47,83]. Considering the shallow-trap model, positrons are collected in the shallow states created by the dilatational strain field[84]. These shallow states act in the same way as the Rydberg states mentioned in the case of negatively charged vacancies. Due to that, positrons can also get detrapped from these shallow states. The relation between κ_{dis} trapping and the δ_{dis} detrapping rate for dislocations is given by[73]

$$\frac{\delta_{dis}}{\kappa_{dis}} = \frac{m^* k_B T}{2 C_{dis} \hbar^2} \mathrm{Erf}\left(\sqrt{\frac{E_{dis}}{k_B T}}\right) \exp\left(-\frac{E_{dis}}{k_B T}\right) \tag{12}$$

where C_{dis} is the dislocation density and E_{dis} is the positron-dislocation binding energy.

In general, at low temperatures (< 100 K), ST contribute more to the average lifetime as they are more effective trapping centers than open-volume defects. As said before, in ST, positrons are also extended into the surrounding bulk and the annihilation parameters are almost equal to that of the perfect lattice (bulk). However, due to the weak binding energy, positrons can be easily detrapped as the temperature increases. Thereby, the detrapped positrons turn into the delocalized state and the fraction of positrons annihilated in ST decreases. Thus, in the case where ST and vacancy defects coexist, the detrapping process results into an increasing average lifetime with temperature. The lifetime related to open-volume defects is always larger than that of the bulk and in consequence, a strong variation in $\bar{\tau}$ is observed. At high enough temperatures, positrons are efficiently detrapped from ST and at that point, they are only annihilated from vacancy states and from the delocalized state. In the case where there is only one vacancy state

for positron annihilation, Eq. (4) adopts the well-known *one-trap model* form,

$$\bar{\tau} = \tau_b \frac{1 + \kappa_v \tau_v}{1 + \kappa_v \tau_b} \tag{13}$$

It is worth noting that this model can only be used at high enough temperatures where the contribution of ST can be neglected.

At low temperatures, the contributions from bulk, vacancies and ST must be taken into account, as positrons can be annihilated in any of the aforementioned three types of states. In the case where only one type of vacancy and ST are present, $\bar{\tau}$ comprises the contribution of the annihilation in the three different states:

$$\bar{\tau} = \tau_b + \frac{\kappa_v(\tau_v - \tau_b)}{\frac{1}{\tau_b} + \kappa_{st} + \kappa_v}. \tag{14}$$

The last expression is the most general one for the case where ST and one type of vacancy are present in the material, where proper annihilation parameters must be chosen for each defect.

V. RESULTS

A. Theoretical calculations

Table I. Calculated positron lifetimes and positron binding energies for the perfect lattice (bulk) and for V_{Se1}, V_{Se2}, V_{Bi} vacancy-type defects in Bi_2Se_3.

	Positron Lifetime (ps)	Binding Energy (eV)
Bulk	225	0.0
V_{Se2}	226	0.013
V_{Se1}	269	0.323
V_{Bi}	251	0.215

Calculations have been performed within ATSUP method for a perfect lattice and for three possible types of vacancy defects in Bi_2Se_3, using a grid of 80^3 points. For the defected lattices, a big enough $(4 \times 4 \times 4)$ supercell has been used to ensure that the density drops to zero at the boundaries. Table I shows the comparison of positron lifetimes for the perfect lattice and for the three types of vacancies: bismuth vacancy (V_{Bi}), the vacancy of selenium located at layers that are bound by VDW forces (V_{Se1}) and the vacancy of selenium located within the QL (V_{Se2}). Only neutral vacancies have been considered.

As shown in Table I, the calculated positron lifetime for defect-free Bi_2Se_3 is 225 ps. In the case of a Bi vacancy its value increases up to 251 ps. Regarding Se vacancies, the obtained lifetime of 226 ps for V_{Se2} is close to the bulk lifetime, while V_{Se1} has a much larger value of 269 ps. This means that non-equivalent Se vacancies are distinguishable by PALS. The lifetime difference can be explained considering two non-equivalent positions of Se atoms.

As shown in Fig. 1, Se1 atoms are located within the layers that are bound by VDW forces. However, Se2 atoms are located within the QL which are strongly bound by covalent forces. The distance between the layers bound by VDW forces is larger comparing to those within the QL. Because of that, the open-volume created for a Se1 vacancy (and in consequence also the related positron lifetime) is much larger than the one of the Se2 and positrons are more localized in Se1 vacancies than in Se2 vacancies.

Regarding the binding energy of positrons (see Table I), the results indicate that V_{Se1} and V_{Bi} act as deep positron traps, with a binding energy of 0.323 eV and 0.215 eV respectively. However, theoretical calculations suggest that positron are weakly bound to V_{Se2} defects, with a binding energy of 13 meV. Due to the low value of the binding energy, V_{Se2} might act as ST. Eventhough proper binding energies must be calculated self-consistently, the comparative results shown in Table I are a guide of the relative trapping depth of positrons in defects.

The obtained positron densities for both perfect and defected Bi_2Se_3 are shown in Fig. 2. In the perfect lattice, the maximum of the positron density is located in the VDW gaps, but when vacancies are present, the positron density is well localized within these defects. The fact that in a perfect lattice, positrons are more confined between the gap of QL demonstrates that positrons are more sensitive to Se1 positions than to the selenium atoms located within the QL. Even considering the presence of Se2 vacancies, the localization of the positrons at V_{Se2} is comparable to the localization of positrons at VDW gap in the perfect lattice.

B. Experimental results

As commented in section Sec. II, three samples of the same composition, Bi_2Se_3, have been used in PALS experiments; as-grown, Q423 and Q473. Q423 and Q473 samples correspond to a Bi_2Se_3 samples that have been annealed to 423 K and 473 K respectively, and afterwards, they have been quenched into ice water.

Fig. 3 shows the temperature evolution of the average positron lifetime in the studied samples. In the as-grown sample, the behavior of the average positron lifetime can be divided in three well-differentiated regions. In the low temperature region, from 15 K to 100 K, $\bar{\tau}$ increases from 251 ps up to 266 ps. In the second region, up to 200 K, the average positron lifetime decreases by about $\approx$ 6 ps. Finally, up to room temperature, $\bar{\tau}$ remains fairly constant at 260 ps. The pronounced temperature dependence indicates the presence of a competition be-

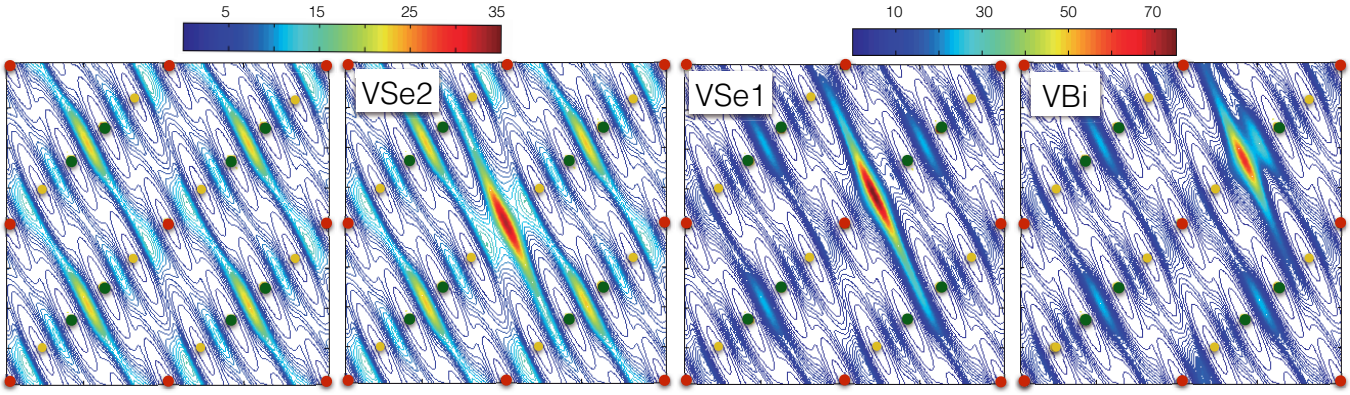

FIG. 2. (Color online). From left to the right, the calculated positron density for Bi_2Se_3 for a perfect lattice (bulk), and a lattice with V_{Se2}, V_{Se1} and V_{Bi} respectively, plane (110). Positions of Se1, Se2 and Bi atoms marked with dots and colored in accordance with Fig 1.

tween open-volume trapping centers (e.g., vacancies) and shallow positron traps[47].

In the temperature range between 100 K and 200 K, the average positron lifetime for the as-grown sample decreases about 6 ps, from 266 ps to 260 ps. At these temperatures, positrons are effectively detrapped from ST and vacancies become the most efficient trapping centers for positrons. So, the decrease in $\bar{\tau}$ has to be attributed to the change in the annihilation parameters of vacancies. However, there are several processes that could explain the observed behavior, for instance: positron detrapping from extended Rydberg states of negatively charged vacancies and the consequent temperature-dependent trapping coefficient ($\kappa_v \propto T^{-1/2}$), and also a change in the charge state of vacancies. Since the fitting provides the most reliable explanation, these hypothesis are discussed further below, in the following section Sec. VI, specifically in VI B.

From 200 K up to room temperature, the average positron lifetime in the as-grown sample remains almost constant. The temperature independent behavior of the average positron lifetime above 200 K, indicates the presence of neutral vacancies.

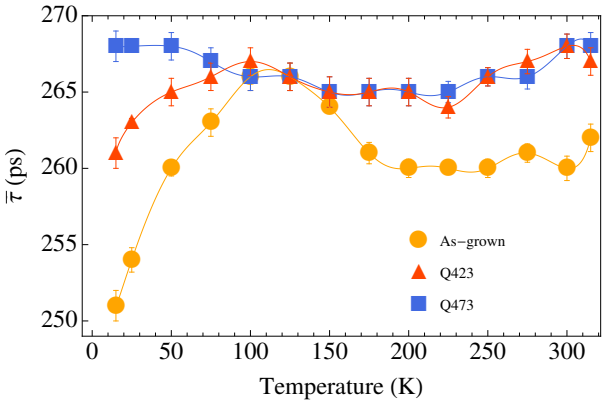

FIG. 3. (Color online). Temperature evolution of the average positron lifetime for the as-grown (orange), and quenched from 423 K (Q423, red) and 473 K (Q473, blue) Bi_2Se_3 sample.

Besides the as-grown sample, the evolution of the $\bar{\tau}$ in Q473 sample shows different features, see Fig. 3. At low temperatures the average lifetime of Q473 sample has a value close to 269 ps, that is significantly longer than the lifetime of 251 ps observed in the as-grown sample. Additionally, as temperature increases, $\bar{\tau}$ decreases. At 125 K, it matches the value of 266 ps measured at the same temperature in the as-grown sample. Afterwards, up to room temperature, $\bar{\tau}$ remains almost constant but fluctuating around 266 ps. Despite of the difference at low temperatures, the average lifetime trend after 125 K is similar to the as-grown sample. However, the $\bar{\tau}$ value differs in about 6 ps. The observed difference between the as-grown and Q473 sample at low temperatures can be easily explained assuming the presence of additional open-volume defects, such as vacancies, that have been retained during the quenching from 473 K. The higher the vacancy concentration, the closer will be $\bar{\tau}$ to the vacancy-related positron lifetime.

Fig. 3 also shows the temperature evolution of $\bar{\tau}$ in sample Q423. The thermal treatment applied to this sample is similar to the one applied to the Q473. However, in the case of Q473 sample, the annealing temperature before quenching has been 423 K, 50 K smaller than the one applied to the other quenched sample. Therefore, one should expect in this case a smaller amount of retained vacancy content than in Q473 sample, but higher than in the as-grown one. At very low temperature, the value of $\bar{\tau}$ in Q423 sample (see Fig. 3) is 260 ps and increases up to 267 ps at around 100 K. In this temperature range, $\bar{\tau}$ shows an intermediate behavior between those of the as-grown and Q473 sample. For higher temperatures, the trend of $\bar{\tau}$ in Q423 sample is very similar to that followed by the Q473.

The temperature dependence of $\bar{\tau}$ in both, as-grown

and Q423 samples, indicates the presence of ST, that act as competing trapping centers to vacancy defects[77]. However, in Q473 sample there is no evidence of the presence of ST. In the quenching process from 473 K, the equilibrium vacancy concentration of that temperature is mostly retained and the concentration is high enough to overtake the ST contribution. Thus, no feature of ST is shown in the PALS spectrum of Q473 sample. However, in the case of Q423 sample, the equilibrium vacancy concentration at 423 K is lower than the one corresponding at 473 K and, as a consequence, the behavior of $\bar{\tau}$ shows again the contribution of ST.

VI. DISCUSSION

A. Identification of defects in Bi_2Se_3

In the as-grown sample, the average positron lifetime shows a strong temperature dependence suggesting the presence of both open-volume defects and defects that act as ST. Decomposition of the average positron lifetime provides detailed information of defects with longer lifetime. However, this decomposition was not feasible. As our theoretical results suggest, the ratio between the shortest and the largest lifetime values, τ_b/τ_{Se1} is $1.19 < (1.3 - 1.5)$ and consequently, it is not enough to perform a reliable lifetime spectrum decomposition. Nevertheless, the temperature evolution of $\bar{\tau}$ gives plenty of information. Although the fitting is more difficult than if $\bar{\tau}$ could be decomposed, it is still possible to fit the data using the general model described in Sec. IV.

In the as-grown sample, at 125 K, $\bar{\tau}$ shows a maximum value of 266 ps, quite close to the 269 ps calculated for the Se1 vacancy. The calculated characteristic lifetimes of V_{Bi} and V_{Se2} are significantly shorter, 251 ps and 226 ps respectively (see Table I). Thereby, the open-volume defects involved at 125 K must be V_{Se1}.

This hypothesis is reinforced by the behavior of $\bar{\tau}$ in Q473 sample. As shown in Fig. 3, at 15 K, the value of the average lifetime of 268 ps is almost exactly the same as the predicted by theoretical calculations for V_{Se1}, 269 ps. Although at low temperatures, ST are much more efficient trapping centers than open-volume defects, a large vacancy concentration could, in principle, overcome the ST component. In this specific case, the influence of the vacancies created by quenching is superimposed and $\bar{\tau}$ rises up to 268 ps. Thus, we can conclude that measured vacancies in the three studied samples are V_{Se1}.

The fact that during quenching V_{Se1} are created can be understood by considering the different binding energies of Se1, Se2 and Bi atoms. Se1 atoms are located in the layers that are bound by VDW forces and this coupling is weaker than the covalent forces which bind the Se2 and Bi atoms. Therefore, the energy needed to create a V_{Se1} has to be lower than for V_{Se2} and V_{Bi}. In a nutshell, the difference in the coupling explains why during quenching V_{Se1} are created instead of V_{Se2} and V_{Bi}. Calculations of defect formation energies performed by other authors[33,41,42] also supports this interpretation.

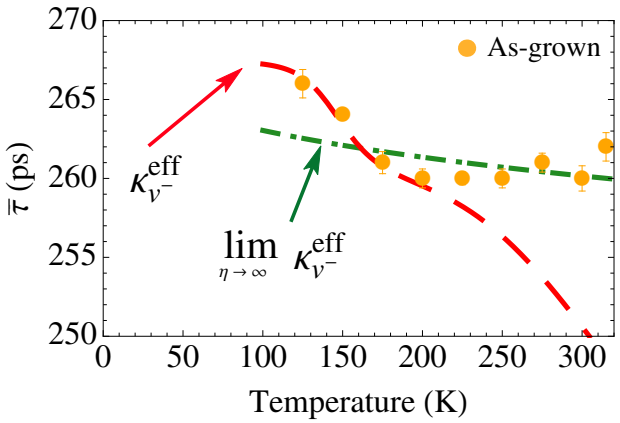

FIG. 4. (Color Online). Fitted $\bar{\tau}$ in high temperature region for the as-grown sample, assuming that V_{Se1} are negatively charged. The red dashed line shows the predicted behavior of the $\bar{\tau}$ considering thermal detrapping from Rydberg states. Green dash-dotted curve shows the evolution of the average positron lifetime in the limit $\eta \to \infty$.

For the as-grown sample, the decrease that $\bar{\tau}$ exhibits in the temperature range from 125 K up to room temperature cannot be explained considering that V_{Se1} are negatively charged. Neither the temperature dependence of negatively charged vacancies nor the detrapping from their Rydberg states can explain the observed behavior of $\bar{\tau}$.

Fig. 4 shows the predicted evolution in the high temperature region of $\bar{\tau}$ considering the presence of negatively charged V_{Se1}^- defects. In this region, the contribution of ST is negligible so Eq. (13) can be used. Eq. (8) describes the effective trapping rate for negatively charged vacancies where positron detrapping from Rydberg states is also taken into account.

On the one hand, positrons trapped at Rydberd states of the vacancy can get detrapped as soon as temperature increases. Although the model that takes into account the detrapping fits quite well in the region 100 K - 200 K (see Fig. 4, red dashed-line), the behavior of the predicted average positron lifetime differs significantly from the experimental results at higher temperatures (200 K - 315 K). As the number of positrons detrapped from Rydberg states increases exponentially, the contribution from V_{Se1}^- decreases in the same amount, resulting in a monotonically decreasing behavior of the calculated $\bar{\tau}$ (Fig. 4, red dashed-line).

On the other hand, as some authors point out[80], if the transition from the Rydberg states to the ground state in the vacancy is fast enough ($\eta \to \infty$), the detrapping effect can be neglected and the effective trapping rate of Eq. (8) turns into Eq. (5) (Fig. 4 green dash-dotted). In this latter case, the trapping rate of negatively charged vacancies depends on temperature and is proportional to $T^{-1/2}$. Thus, as temperature increases,

the effective trapping rate at V^{-}_{Se1} should decrease and, in consequence, the average lifetime also should decrease. However, the slope of $T^{-1/2}$ is quite far from the experimental one in the temperature region from 125 K to 200 K.

Thus, the presence of negatively charged V_{Se1} cannot explain the behavior of $\bar{\tau}$ in the as-grown Bi_2Se_3 sample, and we can conclude that at low temperatures, the charge of the Se1 vacancy has to be neutral.

Nevertheless, the indication of the presence of the neutrally charged vacancies is often the lack of temperature dependence in $\bar{\tau}$. Then, the sudden decrease of $\bar{\tau}$ between 100 K and 200 K can only be explained assuming that Se1 vacancies suffer a charge-state transition from neutral to positively charged, $V^{0}_{Se1} \rightarrow V^{+}_{Se1}$. In order to analyze the data in which the variation on the charge state of V_{Se1} is taking place, the trapping rate must be modified and Eq. (10) turns into $\kappa^{0}_{v} = f(\epsilon)\mu^{0}_{v}C^{0}_{v}$. As the charge state is related to the Fermi distribution from Eq. (9), the higher the temperature, the larger the amount of defects that will ionize to the positive charge state.

The temperature behavior of $\bar{\tau}$ in the as-grown and Q423 sample below 100 K is a telltale sign of the presence of ST. It indicates that, in addition of V_{Se1} defects, additional native defects also coexist in as-grown Bi_2Se_3. The increase of $\bar{\tau}$ from 15 K to 125 K is due to the competition between the V_{Se1} defects and defects that act as ST. Thus, in order to fit the data, the most general expression, that is Eq. (14), has to be employed. In this equation, theoretically calculated values for $\tau_b = 225$ ps and $\tau_v = 269$ ps have been used. The expression for κ^{0}_{v} trapping-rate used for neutral vacancies at low temperatures is the same as the one used for high temperature regime, $\kappa^{0}_{v} = f(\epsilon)\mu^{0}_{v}C^{0}_{v}$.

Related to ST, in the case of non-open volume defects, the effective trapping rate is given by Eq. (11). However, in the as-grown and Q423 sample, it was not possible to fit the low-temperature region using the latter expression which takes into account the detrapping phenomena for ST without open volume defects. As anti-site do not possess any open volume, it is reasonable to think that negatively charged Bi_{Se} and Se_{Bi} anti-site defects cannot be the source of the ST contribution. On the other hand, theoretical calculations suggest that V_{Se2} vacancies might act also as ST due to low binding energy of positrons, and also because the related positron lifetime is very close to the one of the perfect lattice. As shown in Table I, the calculated lifetime difference between the bulk and V_{Se2} is 1 ps.

However, the vacancy concentration ratio between V_{Se1} and V_{Se2} would not be consistent with the calculated defect formation energies if the source of ST would be V_{Se2} defect. The concentration of vacancies (C_v) can be estimated according to Boltzmann distribution by means of $C_v = N\exp(-E_f/k_BT)$, where N is the concentration of atomic site where the defect can be incorporated and E_f the formation energy of the defect[42]. Using the formation energies of V_{Se1} and V_{Se2} from Ref. [42], the ratio of C_{Se1}/C_{Se2} at room temperature is $\approx 10^5$. This means that the concentration of V_{Se2} would be of the order of magnitude $\approx 10^{12}\text{cm}^{-3}$ that is out of the sensitivity range of positron techniques. Thus, V_{Se2} cannot be the source of ST.

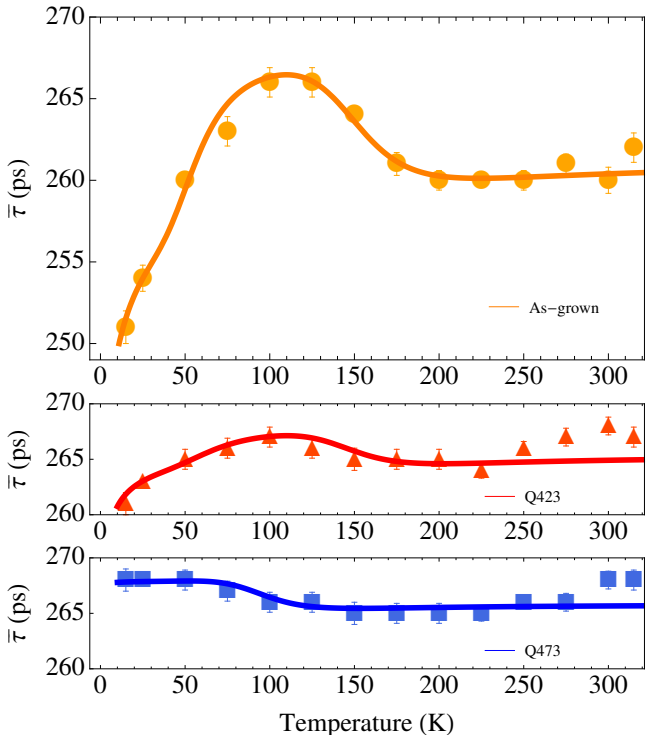

FIG. 5. (Color Online). Fitted data for as-grown, Q423 and Q473 samples.

In fact, the low temperature region for the as-grown and Q423 samples can only be fitted assuming one κ^{eff}_{st} analogous to Eq. (7). This means that ST might be characterized with a very small open volume that is related to a small binding energy of the positron to the defect. The strong temperature dependence of $\bar{\tau}$ indicates that positrons are thermally detrapped from ST. After attempting several models, the best fit has been obtained considering a trapping-detrapping ratio for ST described by Eq. (12).

B. Fitting Process

Fitted results for as-grown, Q423 and Q473 samples are shown in Fig. 5 and parameters obtained by the fitting process are listed in Table II. The best fit of $\bar{\tau}$ for the three samples has been obtained considering on the one hand, the presence of ST, and on the other hand, considering open-volume defects (V_{Se1}) that suffer $V^{0}_{Se1} \rightarrow V^{+}_{Se1}$ charge state transition.

In the fitting process the specific trapping coefficient

Table II. Results obtained from the fitting process in the as-grown, Q423 and Q473 samples.

	V_{Se1} Vacancy Defect		Dislocations		
	C_v(125 K) (cm^{-3})	C_v(315 K) (cm^{-3})	E_{st} (meV)	C_{dis} (cm^{-2})	μ_{st}(20K)(s^{-1})
As-grown	5.3×10^{17}	3.1×10^{16}	22	3.5×10^{10}	1.3×10^{16}
Quenched 423 K (Q423)	1.0×10^{18}	9.0×10^{16}	20	2.1×10^{10}	1.3×10^{16}
Quenched 473 K (Q473)	2.0×10^{19}	1.1×10^{17}	23	2.5×10^{10}	1.0×10^{16}

used for neutral vacancies has been $5{\times}10^{15}$ s^{-1}, consistent with the values in the literature[72,74]. The decrease that $\bar{\tau}$ exhibits in the temperature range from 125 K up to 200 K for the as-grown sample can only be explained under the assumption that the concentration of neutrlly charged V_{Se1} vacancies varies as the temperature increases (see Fig. 3). The neutral vacancy concentration in the as-grown Bi_2Se_3 at low temperatures is 5.3×10^{17} cm^{-3} and due to a charge delocalization, the concentration of neutrally charged vacancies decreases down to 3.1×10^{16} cm^{-3} at room temperature.

The model used for ST in order to fit the low temperature regime, is compatible with the shallow-trap model considered for dislocations. Indeed, an effective trapping rate analogous to the one provided by Eq. (7) for ST, has been applied in the case of dislocations[82,85]. This model predicts values of positron lifetime between the one of the bulk and the one related to typical monovacancies[47,86]. This fact would explain the intermediate measured value of 251 ps at 15 K (between bulk lifetime, 225 ps and V_{Se1}, 269 ps) that $\bar{\tau}$ shows in the as-grown Bi_2Se_3 sample. Moreover, the best fit has been obtained assuming that ST are negatively charged that is in a good agreement with the fact that in most of n-type or undoped semiconductors, dislocations are usually negatively charged[85]. The fitting and the obtained results suggest that the source of ST might be negatively charged dislocations although more studies should be performed to further confirmation. The presence of dislocations in Bi_2Se_3 have been reported in previous works and they can be used to enhance or destroy the Dirac states by their induced strain[50,51]. Moreover, dislocation lines are associated with one-dimensional fermionic excitations in a TI[49].

Under the assumption that the source of ST might be negatively charged dislocations, and considering that dislocations are a chain of spherical scattering centers[50,87], the performed fit leads to a C_{dis} dislocation density ranging between $3.5 - 2.1 \times 10^{10}$ cm^{-2} for the as-grown and quenched samples, see Table II. These values are consistent with the dislocation density ($\approx 10^9$ cm^{-2}) reported in Bi_2Se_3 by previous works[88].

The μ_{st} specific trapping rate for ST obtained from the fit is $\mu_{st} \propto 10^{16}$ s^{-1} in the three samples, which is the typical value for negatively charged defects[47]. Additionally, the value of the positron binding energy of the ST for the three samples is around 20 meV, very close for the expected ST in general (< 0.1 eV), and in particular, for dislocations, because the related open volume is supposed to be rather small. In summary, if the source of ST are dislocations, the obtained results indicate that the annihilation parameters related with dislocations as well as their concentration do not change significantly among the three studied samples.

However, the obtained V^0_{Se1} neutral vacancy concentration at 125 K in the as-grown, Q423 and Q473 samples are 5.3×10^{17} cm^{-3}, 1.0×10^{18} cm^{-3} and 2.0×10^{19} cm^{-3} respectively, and they change to 3.1×10^{16} cm^{-3}, $9.0{\times}10^{16}$ cm^{-3} and $1.1{\times}10^{17}$ cm^{-3} at room temperature. Thus, only by considering a change in the V^0_{Se1} concentration, it is possible to model the temperature evolution of $\bar{\tau}$ for these three samples. This indicates that the change in all three spectra comes from the vacancy-related annihilation parameters.

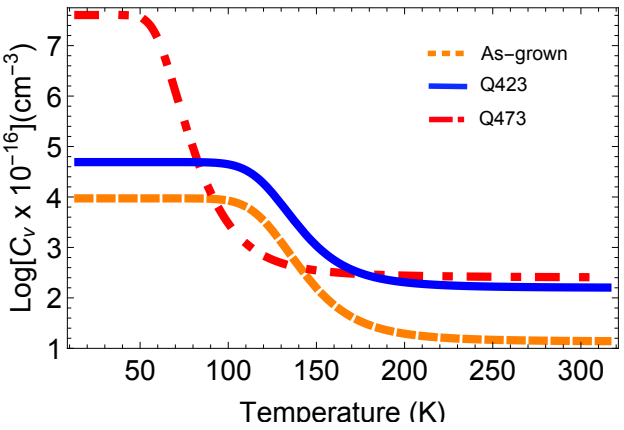

FIG. 6. (Color Online). Evolution of neutrally charged vacancy concentration for as-grown (dashed line), Q423 (solid line) and Q473 (dash-dotted) samples. The decrease of the V^0_{Se1} concentration indicates that some of neutrally charged vacancies have become positively charged due to the charge delocalization.

The observed charge delocalization could also explain the reported concentration of free carriers in Bi_2Se_3. Each ionized selenium vacancy can contribute with one or two electrons to the bulk conductivity. Even though, by PALS it is not possible to know if one or two electrons are ionized from V_{Se1}, we can estimate the lower and the upper bound of V_{Se1} contribution to the bulk conductivity. In the case where vacancies are doubly ionized, the resulting contribution of n_e carrier concentration is proportional to the ionized vacancy concentration C^*_v as $n_e = 2 \times C^*_v$, where the factor two accounts for the two

ionized electrons from each vacancy. On the other hand, when vacancies are single ionized, their contribution to the n-type conductivity has the same value as the ionized vacancy concentration.

Considering the vacancy concentration measured by PALS from which the charge has been delocalized, it leads to a contribution to the carrier concentration ranging between 5×10^{17} cm^{-3} and 3.9×10^{19} cm^{-3}. These values are in good agreement with the reported carrier concentrations obtained by transport measurements and by Hall effect[19,89–91], which range between 2×10^{17} cm^{-3} and 3×10^{19} cm^{-3}.

The variation of V^0_{Se1} neutral vacancies resulted from the fitting process for the three samples are shown in Fig. 6. These values are in a good agreement with previous reports[19,92], although here there is a change in the V^0_{Se1} concentration as the temperature increases. This does not mean that the vacancies are annealing or disappearing. With increasing temperature, vacancies which suffer the transition to the positively charged state, are no longer detectable for positrons as they do not act as positron trapping centers. This reduction of V^0_{Se1} vacancies is related with the factor $f(\epsilon)$ of Eq. (9).

In order to fit the observed ionization process, a temperature dependent $\epsilon_f(T)$ fermi level must be considered in which the energy difference between the defect energy level ϵ_d and the Fermi level ϵ_f varies about ≈ 300 meV from 15 K up to 315 K. As temperature increases, the contribution of native defects affects the pinning of ϵ_f. For the ϵ_d energy of V_{Se1} level the value of 0.079 eV below the conduction band minimum reported in Ref. [42] has been used. The degeneracy factor g of Eq. (9) has been set as $g = 1$, because neutral vacancy defects have no spin degeneracy as they have no bound carriers[75]. Such a change in $\epsilon_f(T)$ has been observed in a previous report[45].

Although it is clear that neutrally charged V_{Se1} vacancies suffer a charge state change, the value of 260 ps in the as-grown sample at room temperature suggests a charge state coexistence of neutrally and positively charged V_{Se1} defects. The charge delocalization process takes place, at least, between 100 K - 200 K. From this temperature, $\bar{\tau}$ remains constant around 260 ps up to room temperature. This average lifetime value is quite far from the one expected for the bulk lifetime of 225 ps. Due to the fact that $\bar{\tau}$ does not depend on temperature in that range, it indicates that neutrally charged vacancies have to be present in Bi_2Se_3 at room temperature. On the whole, the results indicate a coexistence of both V^0_{Se1} and V^+_{Se1} defects in the temperature range of 125 K - 315 K and confirms the role that V_{Se1} have in the origin of n-type doping in Bi_2Se_3 because the observed charge delocalization process.

VII. SUMMARY AND CONCLUSION

By means of positron annihilation lifetime spectroscopy we have characterized the native defects in Bi_2Se_3 from a combined theoretical and experimental study. Our results confirm that more than one type of defects are present. A temperature study of the positron annihilation lifetime for the as-grown sample clearly indicates the presence of both ST and open-volume defects. Although the source of the defects that act as ST has not been conclusively determined, a shallow-trap model for dislocations fits quite well the experimental data, suggesting that dislocations would be the source of these ST. Besides, no direct detection of negatively charged anti-sites defects acting as ST has been observed in PALS experiments suggesting that anti-site defects might not be negatively charged or in a not enough concentration to overcome their contribution at low temperatures.

Moreover, theoretical calculations point out that the two non-equivalent selenium vacancies in Bi_2Se_3 are clearly differentiated by their related positron annihilation lifetime and consequently identification of the proper selenium vacancies present has been possible.

Finally, we have demonstrated that, due to the charge delocalization, at least in the temperature range from 125 K up to 315 K two charge states of selenium vacancies (V^0_{Se1} and V^+_{Se1}) coexist. This result confirms the role of V_{Se1} defects in the n-type nature of Bi_2Se_3 and quantize how the charge is delocalized from these vacancies as temperature increases.

ACKNOWLEDGEMENTS

This work is supported for the Basque Government Grant IT-443-10 and partially supported by the Spanish Ministry of Economy and Competitiveness (MINECO) under the project TEC2014-60173 and by the Generalitat Valenciana under the projects Prometeo II 2015/004 and ISIC/2012/008. I. Unzueta also wants to acknowledge financial support from the Basque Government Grant PRE-2014-214. V. Marín-Borrás thanks the University of Valencia for its pre-doctoral fellowships. Finally we would also like to thank BCMaterials for its economic support.

* iraultza.unzueta@ehu.eus
† nerea.zabala@ehu.eus
‡ vicente.marin-borras@uv.es
§ vicente.munoz@uv.es
¶ joseangel.garcia@ehu.eus
** fernando.plazaola@ehu.eus

[1] C. L. Kane and E. J. Mele, Phys. Rev. Lett. **95**, 146802 (2005).
[2] C. L. Kane and E. J. Mele, Phys. Rev. Lett. **95**, 226801 (2005).

[3] B. A. Bernevig and S.-C. Zhang, Phys. Rev. Lett. **96**, 106802 (2006).
[4] B. A. Bernevig, T. L. Hughes, and S.-C. Zhang, Science **314**, 1757 (2006).
[5] J. E. Moore and L. Balents, Phys. Rev. B **75**, 121306 (2007).
[6] L. Fu, C. L. Kane, and E. J. Mele, Phys. Rev. Lett. **98**, 106803 (2007).
[7] H. Zhang, C.-X. Liu, X.-L. Qi, X. Dai, Z. Fang, and S.-C. Zhang, Nat. Phys. **5**, 438 (2009).
[8] M. König, S. Wiedmann, C. Brune, A. Roth, H. Buhmann, L. W. Molenkamp, X.-L. Qi, and S.-C. Zhang, Science **318**, 766 (2007).
[9] D. Hsieh, D. Qian, L. Wray, Y. Xia, Y. S. Hor, R. J. Cava, and M. Z. Hasan, Nature **452**, 970 (2008).
[10] Y. L. Chen, J. G. Analytis, J.-H. Chu, Z. K. Liu, S.-K. Mo, X. L. Qi, H. J. Zhang, D. H. Lu, X. Dai, Z. Fang, S. C. Zhang, I. R. Fisher, Z. Hussain, and Z.-X. Shen, Science **325**, 178 (2009).
[11] A. A. Taskin and Y. Ando, Phys. Rev. B **80**, 085303 (2009).
[12] Y. Xia, D. Qian, D. Hsieh, L. Wray, A. Pal, H. Lin, A. Bansil, D. Grauer, Y. S. Hor, R. J. Cava, and M. Z. Hasan, Nat. Phys. **5**, 398 (2009).
[13] A. Nishide, A. A. Taskin, Y. Takeichi, T. Okuda, A. Kakizaki, T. Hirahara, K. Nakatsuji, F. Komori, Y. Ando, and I. Matsuda, Phys. Rev. B **81**, 041309 (2010).
[14] D. Hsieh, Y. Xia, D. Qian, L. Wray, J. H. Dil, F. Meier, J. Osterwalder, L. Patthey, J. G. Checkelsky, N. P. Ong, A. V. Fedorov, H. Lin, A. Bansil, D. Grauer, Y. S. Hor, R. J. Cava, and M. Z. Hasan, Nature **460**, 1101 (2009).
[15] D. Hsieh, Y. Xia, L. Wray, D. Qian, A. Pal, J. H. Dil, J. Osterwalder, F. Meier, G. Bihlmayer, C. L. Kane, Y. S. Hor, R. J. Cava, and M. Z. Hasan, Science **323**, 919 (2009).
[16] Z.-H. Pan, E. Vescovo, A. V. Fedorov, D. Gardner, Y. S. Lee, S. Chu, G. D. Gu, and T. Valla, Phys. Rev. Lett. **106**, 257004 (2011).
[17] X.-L. Qi and S.-C. Zhang, Rev. Mod. Phys. **83**, 1057 (2011).
[18] M. Z. Hasan and C. L. Kane, Rev. Mod. Phys. **82**, 3045 (2010).
[19] J. G. Analytis, J.-H. Chu, Y. Chen, F. Corredor, R. D. McDonald, Z. X. Shen, and I. R. Fisher, Phys. Rev. B **81**, 205407 (2010).
[20] M. Neupane, S.-Y. Xu, L. A. Wray, A. Petersen, R. Shankar, N. Alidoust, C. Liu, A. Fedorov, H. Ji, J. M. Allred, Y. S. Hor, T.-R. Chang, H.-T. Jeng, H. Lin, A. Bansil, R. J. Cava, and M. Z. Hasan, Phys. Rev. B **85**, 235406 (2012).
[21] T. Zhang, P. Cheng, X. Chen, J.-F. Jia, X. Ma, K. He, L. Wang, H. Zhang, X. Dai, Z. Fang, X. Xie, and Q.-K. Xue, Phys. Rev. Lett. **103**, 266803 (2009).
[22] Z. Alpichshev, J. G. Analytis, J.-H. Chu, I. R. Fisher, Y. L. Chen, Z. X. Shen, A. Fang, and A. Kapitulnik, Phys. Rev. Lett. **104**, 016401 (2010).
[23] A. A. Taskin, Z. Ren, S. Sasaki, K. Segawa, and Y. Ando, Phys. Rev. Lett. **107**, 016801 (2011).
[24] D. Kim, S. Cho, N. P. Butch, P. Syers, K. Kirshenbaum, S. Adam, J. Paglione, and M. S. Fuhrer, Nat. Phys. **8**, 459 (2012).
[25] L. He, F. Xiu, X. Yu, M. Teague, J. Wanjun, Y. Fan, X. Kou, M. Lang, Y. Wang, G. Huang, N.-C. Yeh, and K. L. Wang, Nano Lett. **12**, 1486 (2012).
[26] J. Chen, H. J. Qin, F. Yang, J. Liu, T. Guan, F. M. Qu, G. H. Zhang, J. R. Shi, X. C. Xie, C. L. Yang, K. H. Wu, Y. Q. Li, and L. Lu, Phys. Rev. Lett. **105**, 176602 (2010).
[27] J. Son, K. Banerjee, M. Brahlek, N. Koirala, S.-K. Lee, J.-H. Ahn, S. Oh, and H. Yang, Appl. Phys. Lett. **103** (2013).
[28] T. Zhang, N. Levy, J. Ha, Y. Kuk, and J. A. Stroscio, Phys. Rev. B **87**, 115410 (2013).
[29] J. Linder, T. Yokoyama, and A. Sudbø, Phys. Rev. B **80**, 205401 (2009).
[30] J. Chang, L. F. Register, S. K. Banerjee, and B. Sahu, Phys. Rev. B **83**, 235108 (2011).
[31] J. Lee, J. Park, J.-H. Lee, J. S. Kim, and H.-J. Lee, Phys. Rev. B **86**, 245321 (2012).
[32] B. Xia, P. Ren, A. Sulaev, P. Liu, S.-Q. Shen, and L. Wang, Phys. Rev. B **87**, 085442 (2013).
[33] Y. S. Hor, A. Richardella, P. Roushan, Y. Xia, J. G. Checkelsky, A. Yazdani, M. Z. Hasan, N. P. Ong, and R. J. Cava, Phys. Rev. B **79**, 195208 (2009).
[34] Z. Ren, A. A. Taskin, S. Sasaki, K. Segawa, and Y. Ando, Phys. Rev. B **84**, 075316 (2011).
[35] G. Wang, X.-G. Zhu, Y.-Y. Sun, Y.-Y. Li, T. Zhang, J. Wen, X. Chen, K. He, L.-L. Wang, X.-C. Ma, J.-F. Jia, S. B. Zhang, and Q.-K. Xue, Adv. Mater. **23**, 2929 (2011).
[36] Z. Ren, A. A. Taskin, S. Sasaki, K. Segawa, and Y. Ando, Phys. Rev. B **85**, 155301 (2012).
[37] P. L. J. Horak, Z. Stary and J. Pancir, J. Phys. Chem. Solid **51**, 1353 (1990s).
[38] S. Urazhdin, D. Bilc, S. H. Tessmer, S. D. Mahanti, T. Kyratsi, and M. G. Kanatzidis, Phys. Rev. B **66**, 161306 (2002).
[39] D. O. Scanlon, P. D. C. King, R. P. Singh, A. de la Torre, S. M. Walker, G. Balakrishnan, F. Baumberger, and C. R. A. Catlow, Adv. Mater. **24**, 2154 (2012).
[40] D. West, Y. Y. Sun, H. Wang, J. Bang, and S. B. Zhang, Phys. Rev. B **86**, 121201 (2012).
[41] S.-X. Wang, P. Zhang, and S.-S. Li, ArXiv e-prints (2012), arXiv:1201.2469 [cond-mat.mtrl-sci].
[42] L. Xue, P. Zhou, C. X. Zhang, C. Y. He, G. L. Hao, L. Z. Sun, and J. X. Zhong, AIP Adv. **3**, 052105 (2013).
[43] J. Bludská, I. Jakubec, S. Karamazov, J. Horák, and C. Uher, J. Solid State Chem. **183**, 2813 (2010).
[44] F.-T. Huang, M.-W. Chu, H. H. Kung, W. L. Lee, R. Sankar, S.-C. Liou, K. K. Wu, Y. K. Kuo, and F. C. Chou, Phys. Rev. B **86**, 081104 (2012).
[45] L.-L. Wang, M. Huang, S. Thimmaiah, A. Alam, S. L. Bud'ko, A. Kaminski, T. A. Lograsso, P. Canfield, and D. D. Johnson, Phys. Rev. B **87**, 125303 (2013).
[46] D. Koumoulis, B. Leung, T. C. Chasapis, R. Taylor, D. King, M. G. Kanatzidis, and L.-S. Bouchard, Adv. Funct. Mat. **24**, 1519 (2014).
[47] H. L. R. Krause-Rehberg, *Positron Annihilation in Semiconductors. Defect Studies*, Vol. 27 (Springer-Verlag, Berlin, 1999).
[48] T. R. Devidas, E. P. Amaladass, S. Sharma, R. Rajaraman, D. Sornadurai, N. Subramanian, A. Mani, C. S. Sundar, and A. Bharathi, EPL (Europhysics Letters) **108**, 67008 (2014).
[49] Y. Ran, Y. Zhang, and A. Vishwanath, Nat. Phys. **5**, 298 (2009).
[50] A. Zhuang, J.-J. Li, Y.-C. Wang, X. Wen, Y. Lin, B. Xiang, X. Wang, and J. Zeng, Angew. Chem. Int. Ed. **53**, 6425 (2014).
[51] Y. Liu, Y. Y. Li, S. Rajput, D. Gilks, L. Lari, P. L. Galindo, M. Weinert, V. K. Lazarov, and L. Li, Nat. Phys. **10**, 294

(2014).
[52] S. Nakajima, J. Phys. Chem. Solids **24**, 479 (1963).
[53] P. Kirkegaard and M. Eldrup, Comput. Phys. Commun. **7**, 401 (1974).
[54] M. Bertolaccini and L. Zappa, Il Nuovo Cimento B Series 10 **52**, 487 (1967).
[55] B. Somieski, T. Staab, and R. Krause-Rehberg, Nucl. Instrum. Method. A. **381**, 128 (1996).
[56] V. Callewaert, K. Shastry, R. Saniz, I. Makkonen, B. Barbiellini, B. A. Assaf, D. Heiman, J. S. Moodera, B. Partoens, A. Bansil, and A. Weiss, ArXiv e-prints (2016), arXiv:1605.06629 [cond-mat.mtrl-sci].
[57] K. Plotkowski, T. Panek, and J. Kansy, Il Nuovo Cimento D **10**, 933 (1988).
[58] I. MacKenzie and J. Fabian, Il Nuovo Cimento B **58**, 162 (1980).
[59] M. A. Monge and J. del Rio, J. Phys. Condens. Matter **6**, 2643 (1994).
[60] R. M. Nieminen, E. Boroński, and L. J. Lantto, Phys. Rev. B **32**, 1377 (1985).
[61] E. Boroński and R. M. Nieminen, Phys. Rev. B **34**, 3820 (1986).
[62] M. J. Puska and R. M. Nieminen, J. Phys. F: Met. **13**, 333 (1983).
[63] J. M. C. Robles, E. Ogando, and F. Plazaola, J. Phys. Condens. Matter **19**, 176222 (2007).
[64] K. O. Jensen, J. Phys. Condens. Matter **1**, 10595 (1989).
[65] B. Barbiellini, M. J. Puska, T. Korhonen, A. Harju, T. Torsti, and R. M. Nieminen, Phys. Rev. B **53**, 16201 (1996).
[66] T. Korhonen, M. J. Puska, and R. M. Nieminen, Phys. Rev. B **54**, 15016 (1996).
[67] G. Kimball and G. Shortley, Phys. Rev. **45**, 815 (1934).
[68] B. Barbiellini and J. Kuriplach, Phys. Rev. Lett. **114**, 147401 (2015).
[69] W. Brandt and R. Paulin, Phys. Rev. B **5**, 2430 (1972).
[70] P. Hautöjarvi, *Positrons in Solids. Topics in Current Physics*, Vol. 12 (Springer, Heidelberg, 1979).
[71] M. Puska and R. Nieminen, Rev. Mod. Phys. **66**, 841 (1994).
[72] M. J. Puska, C. Corbel, and R. M. Nieminen, Phys. Rev. B **41**, 9980 (1990).
[73] M. Manninen and R. Nieminen, Appl. Phys. A **26**, 93 (1981).
[74] C. C. K. Sarinen, P. Hautojärvi, *Semiconductors and Semimetals* (Academic Press, New York, 1998) p. 209.
[75] M. C. K. Edmund G. Seebauer, *Charged Semiconductor Defects* (Springer-Verlag London Limited, 2009).
[76] R. Krause-Rehberg, A. Polity, W. Siegel, and G. Kuhnel, Semicond. Sci. Technol **8**, 290 (1993).
[77] K. Saarinen, P. Hautojärvi, A. Vehanen, R. Krause, and G. Dlubek, Phys. Rev. B **39**, 5287 (1989).
[78] C. Corbel, F. Pierre, K. Saarinen, P. Hautojärvi, and P. Moser, Phys. Rev. B **45**, 3386 (1992).
[79] F. Plazaola, K. Saarinen, L. Dobrzynski, H. Reniewicz, F. Firszt, J. Szatkowski, H. Meczynska, S. Legowski, and S. Chabik, J. Appl. Phys. **88**, 1325 (2000).
[80] A. Zubiaga, F. Plazaola, J. A. García, F. Tuomisto, V. Muñoz-Sanjosé, and R. Tena-Zaera, Phys. Rev. B **76**, 085202 (2007).
[81] E. Hashimoto and T. Kino, J. Phys. Soc. Jpn **60**, 3167 (1991).
[82] L. C. Smedskjaer, M. Manninen, and M. J. Fluss, J. Phys. F: Met. **10**, 2237 (1980).
[83] Y. Kamimura, T. Tsutsumi, and E. Kuramoto, Phys. Rev. B **52**, 879 (1995).
[84] A. Kawasuso, M. Suezawa, M. Hasegawa, S. Yamaguchi, and K. Sumino, Jpn. J. Appl. Phys. **34**, 4579 (1995).
[85] H. S. Leipner, C. G. Hübner, T. E. M. Staab, M. Haugk, and R. Krause-Rehberg, Phys. Status Solidi A **171**, 377 (1999).
[86] H. Häkkinen, S. Mäkinen, and M. Manninen, Phys. Rev. B **41**, 12441 (1990).
[87] M. A. Abdel-Rahman, E. A. Badawi, and S. K. Abdel-Raheem, Proceedings of the 3th Radiation Phys. Conf. **1**, 168 (1996).
[88] H. D. Li, Z. Y. Wang, X. Kan, X. Guo, H. T. He, Z. Wang, J. N. Wang, T. L. Wong, N. Wang, and M. H. Xie, New J. Phys. **12**, 103038 (2010).
[89] A. Segura, V. Panchal, J. F. Sánchez-Royo, V. Marín-Borrás, V. Muñoz-Sanjosé, P. Rodríguez-Hernández, A. Muñoz, E. Pérez-González, F. J. Manjón, and J. González, Phys. Rev. B **85**, 195139 (2012).
[90] Z. Wang, T. Lin, P. Wei, X. Liu, R. Dumas, K. Liu, and J. Shi, Appl. Phys. Lett. **97**, 042112 (2010).
[91] J. Suh, D. Fu, X. Liu, J. K. Furdyna, K. M. Yu, W. Walukiewicz, and J. Wu, Phys. Rev. B **89**, 115307 (2014).
[92] N. P. Butch, K. Kirshenbaum, P. Syers, A. B. Sushkov, G. S. Jenkins, H. D. Drew, and J. Paglione, Phys. Rev. B **81**, 241301 (2010).